BİLİMSEL MADENCİLİK DERGİSİ
SCIENTIFIC MINING JOURNAL
TMMOB Maden Mühendisleri Odası Yayını / The Publication of the Chamber of Mining Engineers of Turkey
www.mining.org.tr

Original Research / Orijinal Araştırma

Analysis of the karst development law based on multiple exploration technologies of Cambrian limestone

Kambriyen kireçtaşının karstlaşma sürecinin farklı araştırma teknolojileri ile analizi

Zhenzi Yu[a,b], Junhao Ren[c], Bo Zhang[a,b], Wei Zhao[c], Junzhi Wang[c], Xinyi Wang[c,d,e,*]

[a] *Energy and Chemical Industry Group of China Pingmei Shenma, Pingdingshan, 467000, CHINA*
[b] *State Key Laboratory of Coking Coal Exploitation and Comprehensive Utilization, Pingdingshan, 467000, CHINA*
[c] *Institute of Resources & Environment, Henan Polytechnic University, Jiaozuo, 454000, CHINA*
[d] *Collaborative Innovation Center of Coalbed Methane and Shale Gas for Central Plains Economic Region, Henan Province, Jiaozuo, 454000, CHINA*
[e] *State Collaborative Innovation Center of Coal Work Safety and Clean-efficiency Utilization, Jiaozuo 54100, CHINA*

Geliş - Received: 11 Ağustos - August 2020 ▪ *Kabul - Accepted:* 01 Aralık - December 2020

A B S T R A C T

Coal mine floor limestone aquifers are a major source of water inrush from the coal seam floor and a serious threat to the safety of coal mining. In order to reduce and avoid the occurrence of water inrush within the coal mine, we use multiple detection techniques, which are geophysical exploration technology, drilling technology, water inrush accidents and tracer test, to develop a multi-faceted exploration of karst development and analyze its development characteristics in the Chaochuan mine No. 1 well. The results show that, the Cambrian limestone (CL) karst water is poor; there is a certain hydraulic connection. Near faults F_5, F_1, F_{125}, and SF_{28}, the area is less water-rich area, and the deep karst water forms a closed area; 61.54 % of shallow water inrush accidents in the Taiyuan limestone and CL karsts were caused by large tectonic and nearby shallow faults. The karst vertical zonation is shallow; the shallow water level decreased more in the West Wing of the No. 1 well than in the East Wing.

Keywords: Transient electromagnetic, Hydrogeology drilling, Water inrush, Borehole water inflow, Dynamic water-level, Tracer test.

Introduction

Water inrush from the coal seam floor has always threatened safe production in mines. The water inrush is not only sudden, but also has a strong impact. In a short time, it can flood wells and bring huge economic losses (Wang et al., 2017; Wang et al., 2016b; Wu et al., 2014). Limestone is often hidden at the base of the coal seam. Due to its karst development, strongly water-rich with good connectivity, limestone is the main water source for the coal seam floor under mining conditions, seriously threatening safe mining of coal (Qiao et al., 2014; Dong, 2010; Yang et al., 2018).

The karst development of the coal seam floor is affected by many factors and has very complex features such as hydraulic connections and water inhomogeneity. How to accurately depict the characteristics of karst development and the water-rich law is a major issue in the study of mine hydrogeology (Wu et al., 2013; Kovàcs et al., 2017). Wang (Wang et al., 2016a; Wang et al., 2018) have studied the water rich characteristics of the Cambrian limestone in the No. 2 well of the Pingdingshan coal field and formulated the related countermeasures for water control by using geological drilling, field connectivity tests, water drainage drilling, water temperature field monitoring, and transient electromagnetic exploration. Dai (2010) studied the influence of geological structures on karst development in the Hancheng mining area and concluded that (1) the structural fissures are dominant in karst development, and (2) the vertical karst development shows a zonal distribution where upper and lower aquifer connectivity is strong. Hao et al. (2013) analyzed the karst development characteristics and influencing factors of the Ordovician limestone in the Gujiao mining area by using the hydrogeological drilling data and their core characteristics, and concluded that the karst development is mainly controlled by the lithologic rhythm combination, resulting in karst phenomenon between the strong and weak phases, where the ground structure raises the stratum and controls the degree of karst development. Hu et al. (2010) applied chemical tracer tests to explore the characteristics of deep karst development in the Qiuji mine and concluded that the karst development in the mine field is not uniform. Most of the areas are strong karst regions, and the karst development in a few regions is mainly characterized by fissure and weak karst development. The above research on the characteristics of karst development and the achievements made in the typical coal mine have laid a scientific foundation for the identification of water inrush sources and the probability of water in-rush occurring, and previous studies have also helped determine the direction for prevention and control of the coal mine water damage, which has important theoretical and practical significance.

*Corresponding author/Sorumlu yazar: wangxy@hpu.edu.cn : https://orcid.org/0000-0002-5275-9209

https://doi.org/10.30797/madencilik.950069

This paper takes the No. 1 well in the Chaochuan mine of Pingdingshan Coal Co.Ltd, Henan Province, China as an example (abbreviated as the No. 1 well). Based on the analysis of the hydrogeological conditions of the mine, geophysical exploration, hydrogeological drilling, water in-rush feature analysis, underground water discharge engineering, dynamic changes of groundwater level, and tracer tests were adopted. A comprehensive analysis of the Cambrian limestone (abbreviated as CL) karst development characteristics of the No. 1 well coal seam floor is performed, and then provide a beneficial reference for the prevention and control of mine water hazards in the future and reduce the probability of water inrush accident in karst aquifer of coal seam floor.

1. Geological overview

Chaochuan mine is located about 15 km south of Chenzhou City in Henan Province. The mine measures about 10 km from east to west and 4 km from south to north, and the mining area is about 21 km^2. The No. 1 well is located in the middle of the Chaochuan mine, with fault F_5 in the north, coal outcrop in the south, fault F_{104} in the southwest, and fault F_1 in the northeast. It accounts for 34.4 % of the total area of the Chaochuan mine (Figure 1).

The main faults of the No. 1 well are located on the northern, western, and southern boundaries of the well field, and a series of northwest (NW) and near east-west (E-W) faults play an important role in the burial and distribution of the CL aquifer on the coal seam floor of the minefield and the discharge of groundwater recharge and runoff (Figure 2).

The F_1 normal fault extends 4,300 m in the No. 1 well and with a drop of 60 m to 130 m. Because the lower CL aquifer of the F_1 fault is connected with the No. 2-1 coal seam in the upper plate, the CL is buried deeper in the lower part, and the karst development is weak. The F_1 fault is a lateral non-conducting fault, or a weak water conducting fault, in the No. 1 well. However, in the fracture zone of the upper wall, there may be a water-rich strip along the strike of the fault. The F_5 normal fault in the No. 1 well intersects the F_4 faults, with an extension of 3,150 m and a drop of 26 m to 118 m. The fault causes the CL in the No. 1 well to stagger along the deep part. It is a non-conducting or weakly conducting boundary for the No. 1 well.

The SF_{28} drop is at 40 m to 130 m, and the extension length is 3,600 m. SF_{28} causes the CL in the south to connect with the coal seams or Carboniferous limestone in the north. Thus, it loses the hydraulic connection with the CL in the north, and the lateral water conductivity of the fault is weak. The runoff of the CL groundwater is blocked northward or northeast (NE), resulting in the formation of a water-rich zone on the southern plane of the fault.

The F_{125} normal fault extends 850 m in the No. 1 well with a drop of 20 m to 70 m. The underground water of the CL, found in the two disks on the East and west sides of the fault, is connected. Therefore, the shallow part belongs to the lateral water diversion fault, while the groundwater hydraulic relations between the two pieces of CL in the deep fault are weak.

The F_{104} normal fault is a fault exposed underground, extending 1,600 m with a drop of 50 m.

The No. 1 well coal-bearing stratum is shown in Figure 3. The leading role of No. 1 well water-filling is the coal seam floor, which consists of the Carboniferous Taiyuan formation thin limestone and Cambrian thick limestone aquifers. The L_{1+2} thin limestone in the Taiyuan formation is generally developed, with an average thickness of about 3.83 m, and it is about 8 m from the bottom of the No.2-1 coal seam. The average thickness of the Cambrian thick limestone is 146.24 m, with an elevation of -100 to -600 m (Figure 2). The aquifer is about 50 m from the bottom of the No. 2-1 coal seam. Due to the well-developed geological faults in the No. 1 well, the karst fissures in the CL aquifer are also well developed as a result of the influence of faults and the floor damage caused by mining. The groundwater is not only the main supply source of the limestone aquifers in the upper Taiyuan group but also the main water filling source of the No. 2-1 coal seam mining.

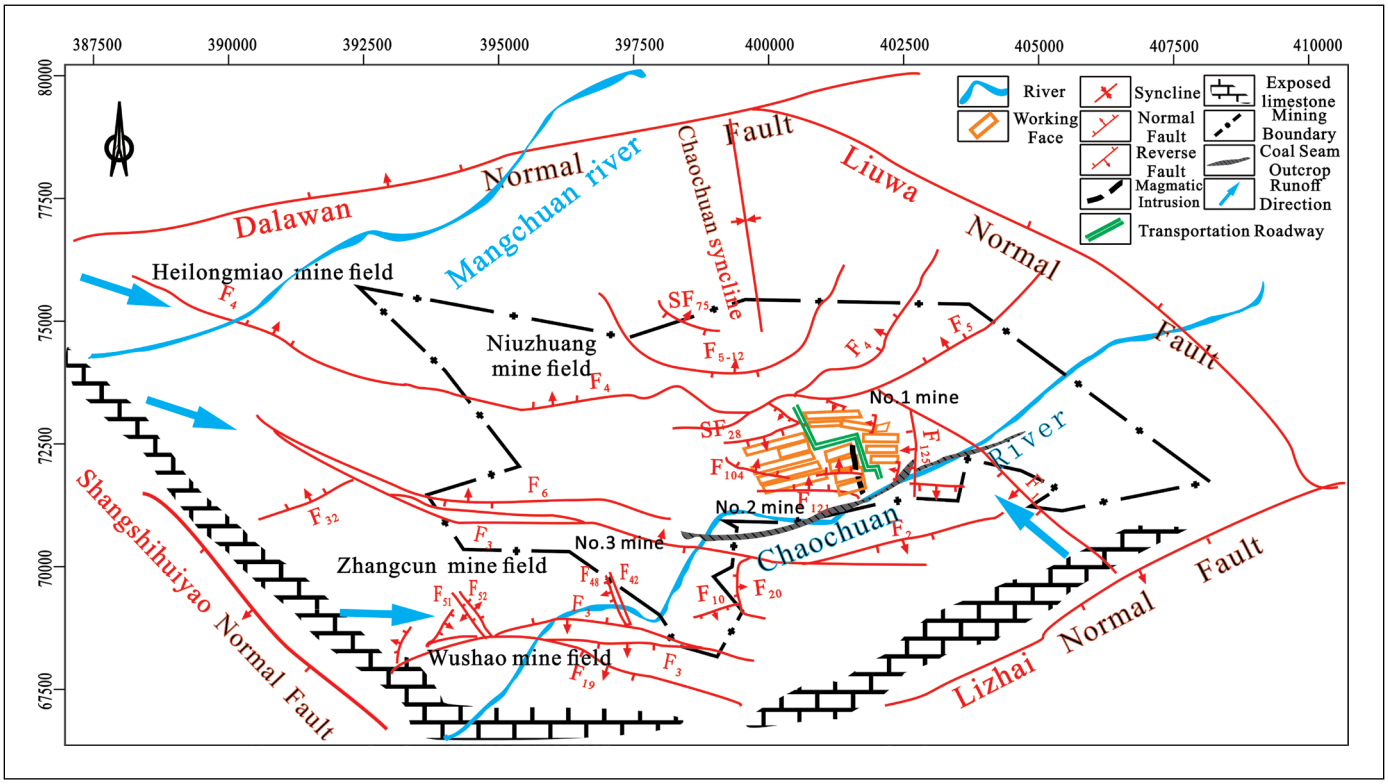

Figure 1. *Main fault and karst water supply diagram of Chaochuan mine*

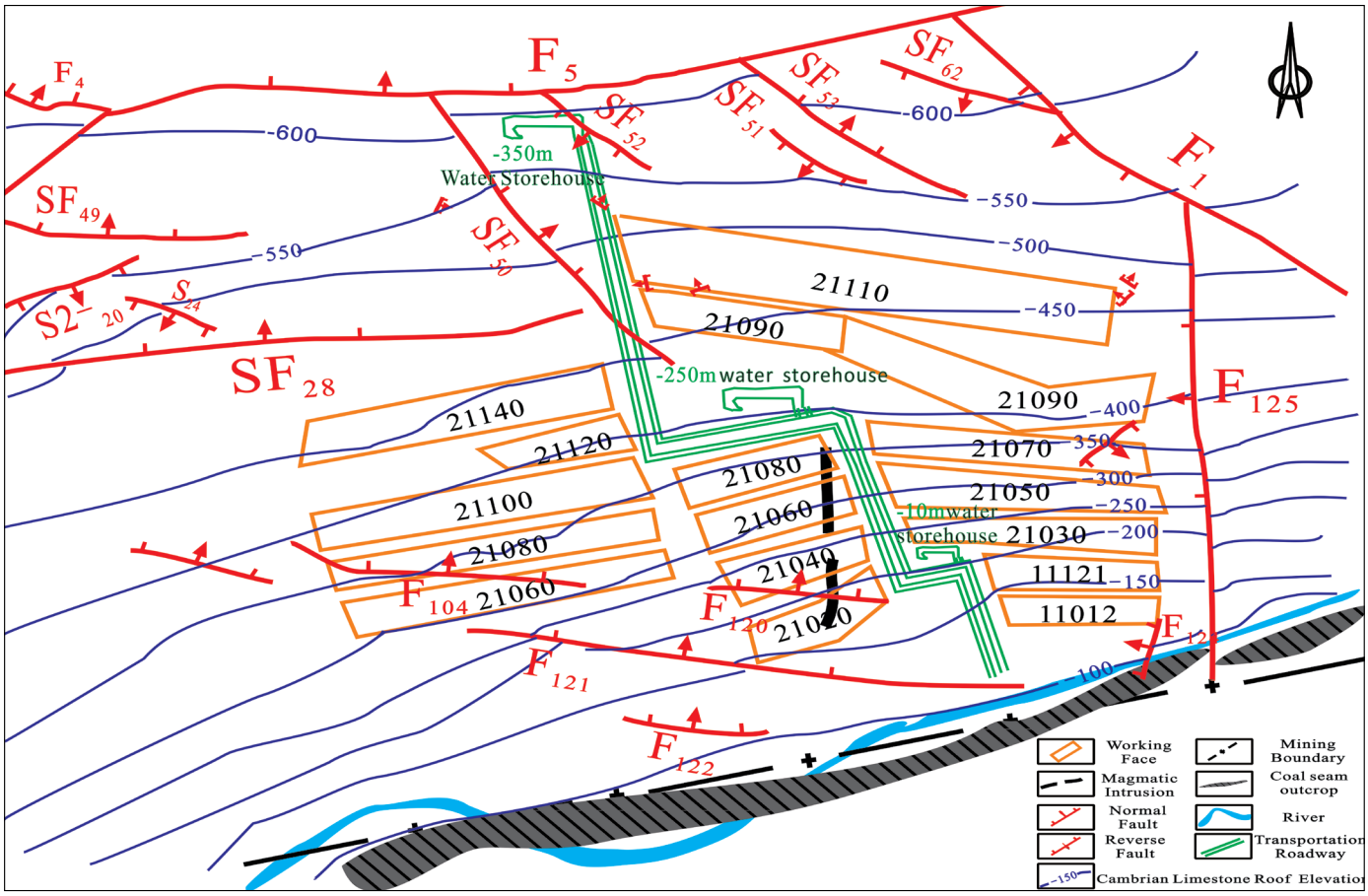

Figure 2. *Cambrian limestone elevation in No. 1 well of Chaochuan mine*

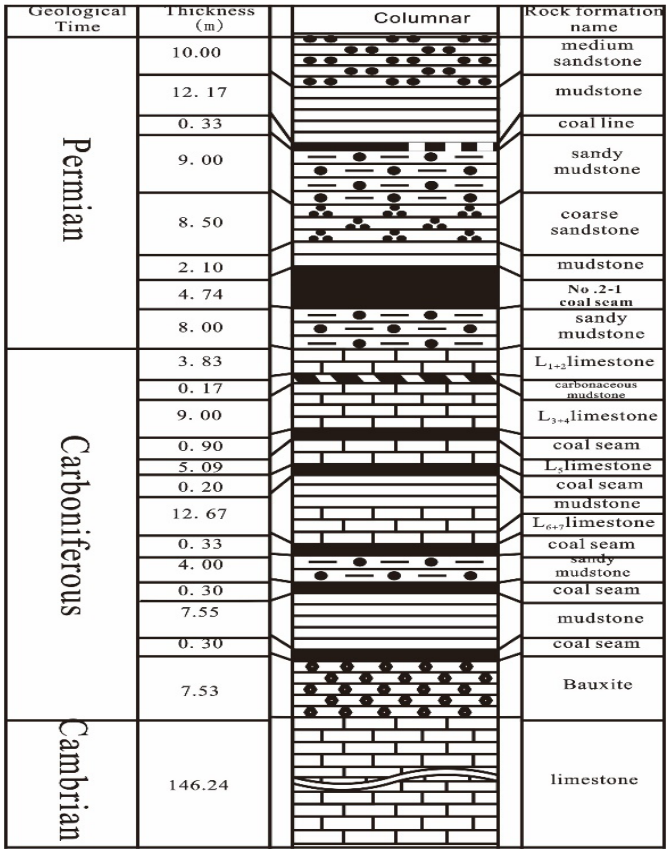

Figure 3. *Coal bearing stratigraphic section: No. 1 well*

2. Transient electromagnetic prospecting

in order to discover the water-rich anomalies of the CL aquifer in the No. 2-1 coal seam, ground transient electromagnetic (Liu et al., 2017; Sun et al., 2013) exploration was carried out within the No. 1 well range. The following exploration range was used: From the F_5 reverse fault southward to -250 m water storehouse, and west from the 13th exploration line eastward to the 5th exploration line. The total area was 3.1 km^2, with a survey line spacing of 40 m × 40 m and a total of 3,184 physical exploration points. The detection depth was set at 80 m in the CL aquifer. According to the transient electromagnetic apparent resistivity, the aquifer was usually divided into 2 levels, rich in water and weak in water (Wang et al., 2016a; Wang et al., 2018). According to the exploration situation in this mine, in the top range of the CL (depth 0~40 m), an apparent resistivity of less than 85 Ω•m was defined as a strong water-rich zone; and in the middle of the CL depth (depth 40~80 m), apparent resistivity less than 90 Ω•m was defined as a strong water-rich area. The survey results are shown in Figure 4.

From Figure 4, the depth of the 0 to 40 m CL has been delineated in 14 low resistivity anomalies, and the depth of the 40 to 80 m CL has been delineated in 16 low resistivity zones. The proportions of the areas occupied by the survey were 17.94 % and 18.42 %, respectively. In addition, the distribution of the low resistivity anomaly areas was sporadic and beaded, and the range of a single low resistivity anomaly was small, which indicated that the CL aquifer in the No. 1 well range had poor water-richness as a whole. In the 0~40 m and 40~80 m depths from the top interface of the CL, there were overlapping regions in the low resistivity anomaly area, which indicated that there was a certain hydraulic connection between the groundwater in the top and the middle sections of the CL aquifer.

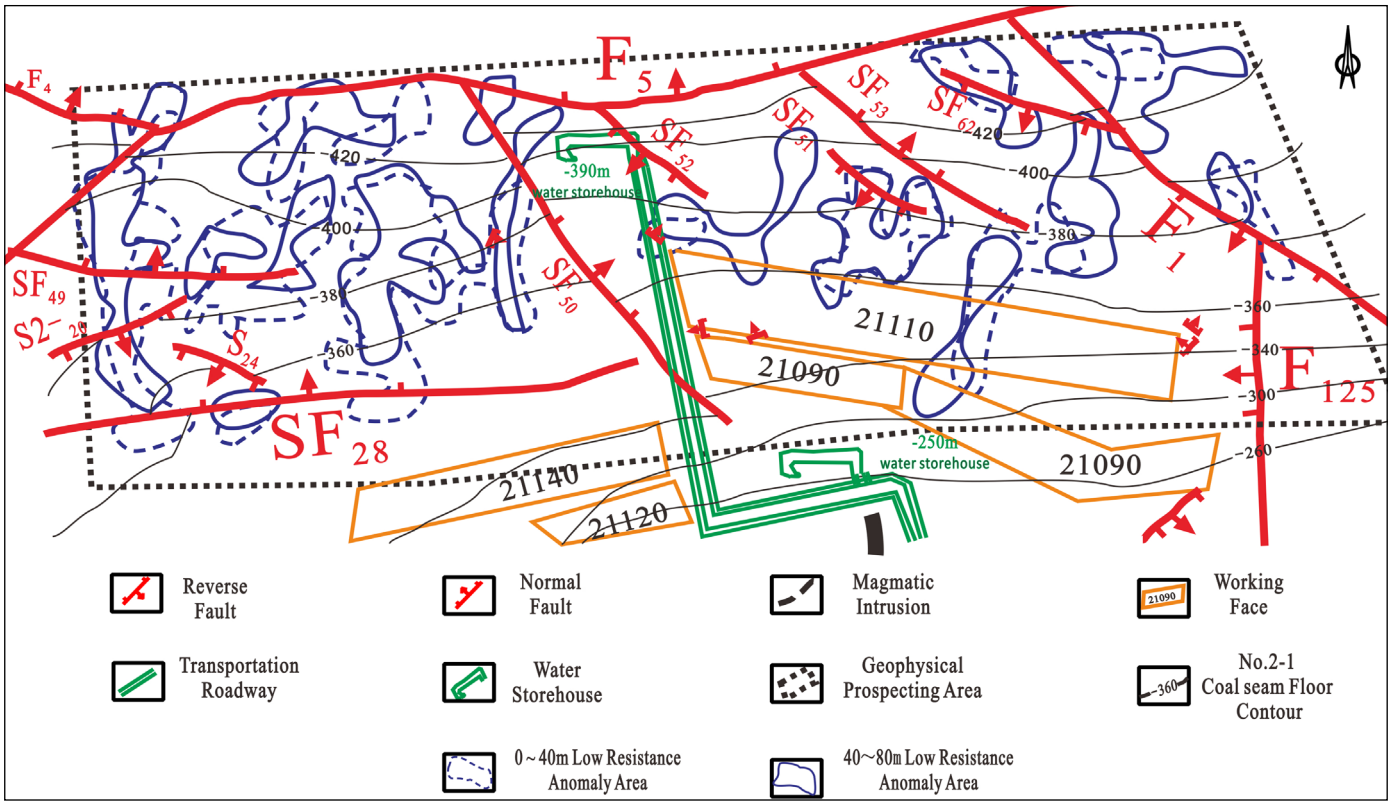

Figure 4. *Deep low resistivity anomaly area distribution of No. 1 well*

In addition, near F_5, F_1, F_{125}, and SF_{28}, the low-resistance anomaly area was sporadic, indicating that these faults were weakly conducting water, which was consistent with the actual situation revealed during the construction of the mine roadway. In addition, due to the weak water conductivity of F_5, F_1, F_{125}, and SF_{28}, the hydraulic connection between the deep and shallow parts of the CL was weak on both sides of the fault. A hydrogeological unit with relatively closed CL aquifer of the No. 1 well was formed.

3. Hydrogeological exploration

During the No. 1 well exploration, 10 geological holes were drilled from the target layer to the CL (Table 1). The drilling depth was between 16.64 and 652.33 m, and the mean value was 342 m. The final borehole elevation was within the range of 250.94~ -415.21 m with a mean value of -106.17 m. The water leakage in all 10 boreholes indicates that the karst fissures in the shallow CL aquifer were generally developed and rich in water.

In the No. 1 well mining process, in order to monitor the groundwater level of the CL aquifer, eight hydrogeological boreholes were constructed at different stages (Table 2). The drilling depth was between 420.20 m and 874.60 m, and the mean value was 555.30 m. The final hole elevation in the borehole ranged from -242.00 m to -693.00 m with an average of -355.69 m. There is no leakage in the 8 boreholes, which indicated that the CL karst in the deep part of the area was weak and not strongly water-rich.

Table 1. *Water leakage of geological boreholes in the CL*

Drilling number	Leakage point position		Water leakage
	Depth(m)	Elevation(m)	
1-101	239.29	-67.38	The exposed thickness of the CL is 56.65 m, and drilling is stopped after leakage
10-97	267.25	-48.44	The exposed thickness of the CL is 104.37 m, and drilling is stopped after leakage
12-21	473.68	-245.66	The exposed thickness of the CL is 38.98 m, and drilling is stopped after leakage
12-96	370.00	-156.88	The exposed thickness of the CL is 44.64 m, and drilling is stopped after leakage
13-93	652.33	-415.21	Revealing the thickness of the CL is the discovery of water leakage, and then terminates drilling
14-91	313.00	-89.94	The exposed thickness of the CL is 34.40 m, and drilling is stopped after leakage
14-92	444.00	-228.93	The exposed thickness of the CL is 12.89 m, and drilling is stopped after leakage
20-23	562.88	-257.07	The exposed thickness of the CL is 82.35 m, and drilling is stopped after leakage
21-88	80.95	196.89	The exposed thickness of the CL is 55.35 m, and drilling is stopped after leakage
27-21	16.64	250.94	The exposed thickness of the CL is 15.45 m, and drilling is stopped after leakage
Mean	342.00	-106.17	The average exposed thickness of the CL is 44.51 m

Table 2. *Hydrogeological borehole of the CL*

Drilling number	Depth(m)	Elevation(m)	Water leakage
Water 1	440.00	-262.00	The revealed thickness of the CL is 61.50 m, and there is no water leakage phenomenon
Water 2	420.20	-242.00	The revealed thickness of the CL is 3.70 m, with rock breaking, there is no leakage phenomenon
Water 3	489.00	-314.00	The revealed thickness of the CL is 13.00 m, there is no water leakage phenomenon
Water 6	495.20	-289.00	The revealed thickness of the CL is 14.60 m, there is no water leakage phenomenon
Water 7	715.20	-468.00	The revealed thickness of the CL is 7.20 m, there is no water leakage phenomenon
Water 8	424.60	-250.00	The revealed thickness of the CL is 85.20 m, rock breaking, there is no leakage phenomenon.
Water 9	874.60	-693.00	The revealed thickness of the CL is 67.50 m, with rock breaking, there is no leakage phenomenon.
4-99	583.62	-327.50	The revealed thickness of the CL is 74 m, karst is not developed
Mean	555.30	-355.69	The average revealed thickness of the CL is 40.84 m

Comparing the boreholes in Table 1 and 2, we see that the borehole depth of the former was much smaller than that of the latter, and the elevation of the final borehole was much higher than that of the latter. For the exposed CL thickness, the former was 44.51 m, and the latter was 40.84 m. The difference between the two was not large, but the leakage situation is very different. This is due to the large amount of groundwater being discharged during the excavation process of the mine, resulting in a drastic decline in the groundwater level of the CL aquifers, which made it impossible to see groundwater in the hydrogeological boreholes of later construction.

4. Water inrush feature analysis

Since 1973, there have been 22 water inrush accidents in the No. 1 well (Figure 5). Eighteen of them were water inrush from the limestone aquifer of the bottom plate, accounting for 81.82 % of total occurrences. There were 13 times where water inrush exceeded 10 m^3/h, and 11 of them where the water inrush originated from the CL aquifer, accounting for 84.62 %. The maximum two water inrush occurrences were 1,440 m^3/h and 1,996 m^3/h, both from the CL aquifer. These results indicated that the most serious threat to No. 1 well mining is the bottom CL aquifer.

For the 13 inrush water incidents with No. 1 well water volume exceeding 10 m^3/h, eight were caused by geological structure (fault and fold), accounting for 61.54 %. For the eight events, seven were water in-rush from the fault and one from the syncline. Figure 5 shows that most of the water in-rush points associated with the fault were located near the fault facing E-W direction, indicating that the structural fracture zone was a zone of karst fissure, which not only controlled the enrichment of the groundwater but also affected the direction of the runoff. Therefore, it was the most prone position for water inrush in the bottom limestone aquifer.

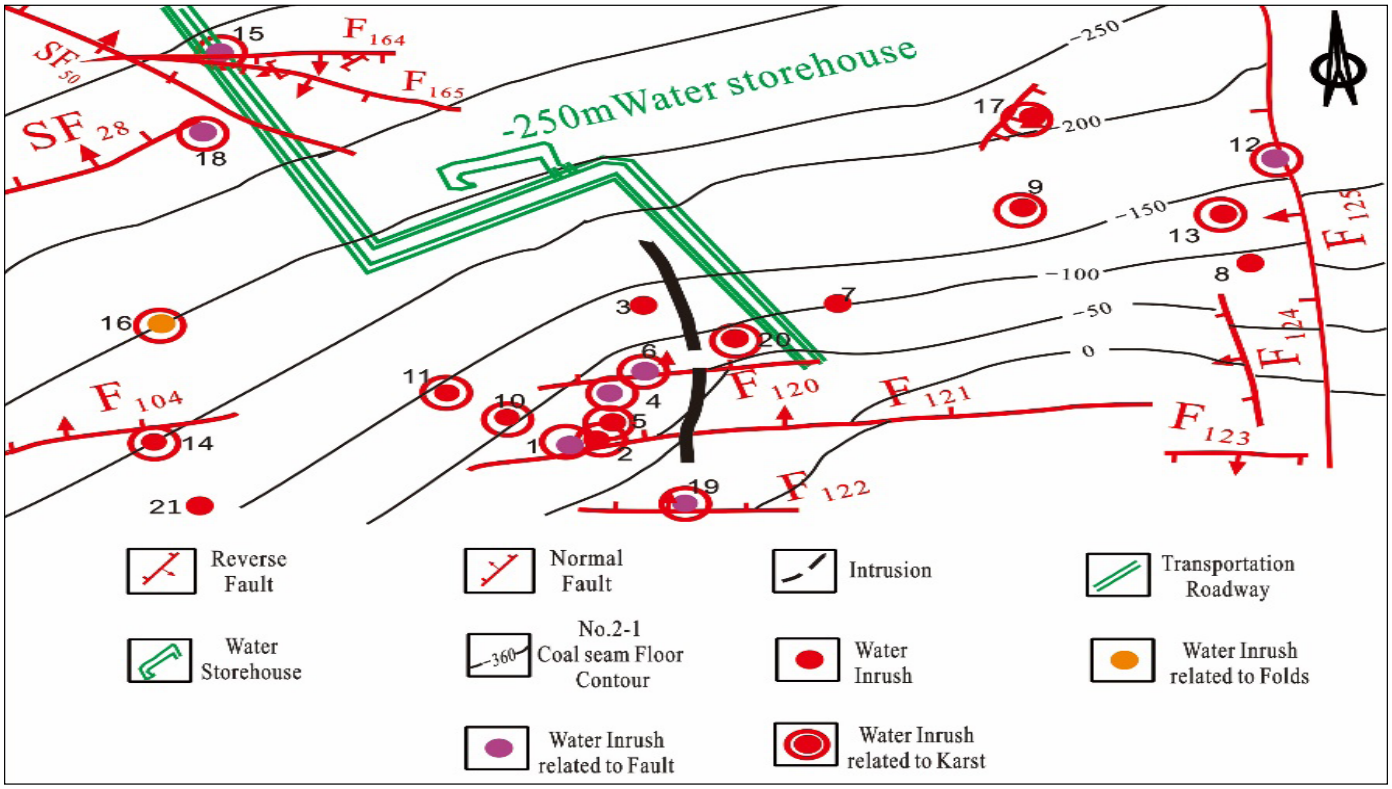

Figure 5. *Distribution diagram of water inrush accidents over the years of No. 1 well.*

Secondly, as shown in Figure 5, there were 18 cases for the water inrush of the limestone aquifer of the No. 2-1 coal seam above -200 m, accounting for 81.82 % of the total water inrush accidents, indicating that the shallow limestone aquifer had more water inrush than the deep part. The incidents were also more concentrated in the vicinity of small faults, which was mainly due to the fact that shallow small faults were more developed than deep ones. In general, the large faults mainly caused the breakage of the regional rock formations, while the minor faults made the surrounding rock mass more broken, resulting in the development of karst fractures. In addition, the fractured rock layer had a large CO_2 content, making the erosion ability stronger and the groundwater circulation in the karst fracture faster, which led to stronger CO_2 erosion ability (Lipar and Webb, 2015). With the increase of depth, the CO_2 recharge in the water was not sufficient, and the groundwater circulation slowed down, which caused the erosion ability of CO_2 to decrease, so that the karst development in the mine field eventually led to zoning in the vertical direction. That is, the shallow karst development was stronger than the deep part (Zhao, 2014; Dai et al., 2017).

Based on the analysis of the water inrush frequency, the shallow karst fracture was more developed than the deep part, which was consistent with the third part.

5. Downhole drainage and decreasing pressure drilling

In order to reduce the underground water level of the limestone aquifer in the Cambrian, which will reduce the threat of water inrush from the floor of the coal seam mining, the special discharge roadways were constructed (Figure 6) according to the mining progress of the No. 1 well, and the drainage and decreasing pressure drilling were built in the roadway (Table 3). According to Table 3, the benefits could be seen from four indices, such as the number of water inrush holes, minimum water inflow, maximum water inflow, and average water inflow. Water inflow must occur in the borehole of the roadway with an elevation of more than -250 m, The minimum, maximum, and average water inflows range from 0.01~16.00 m^3/h, 150.00~232 m^3/h, and 84.28~90.00 m^3/h, respectively, The proportions of water in-rush drilling, minimum water inflow, maximum water inflow, and average water inflow in the roadway with elevations below -300 m range from 40.74~100 %, 0.00~1.00 m^3/h, 3.00~90.00 m^3/h, and 2.00~17.61 m^3/h, respectively. Obviously, the former four indicators were far better than the latter, reflecting that the karst development of the limestone aquifers of the deep Cambrian in the deep No. 1 well was weaker than that in the shallow, which was completely consistent with the results from the previous analysis in Sections 3 and 4.

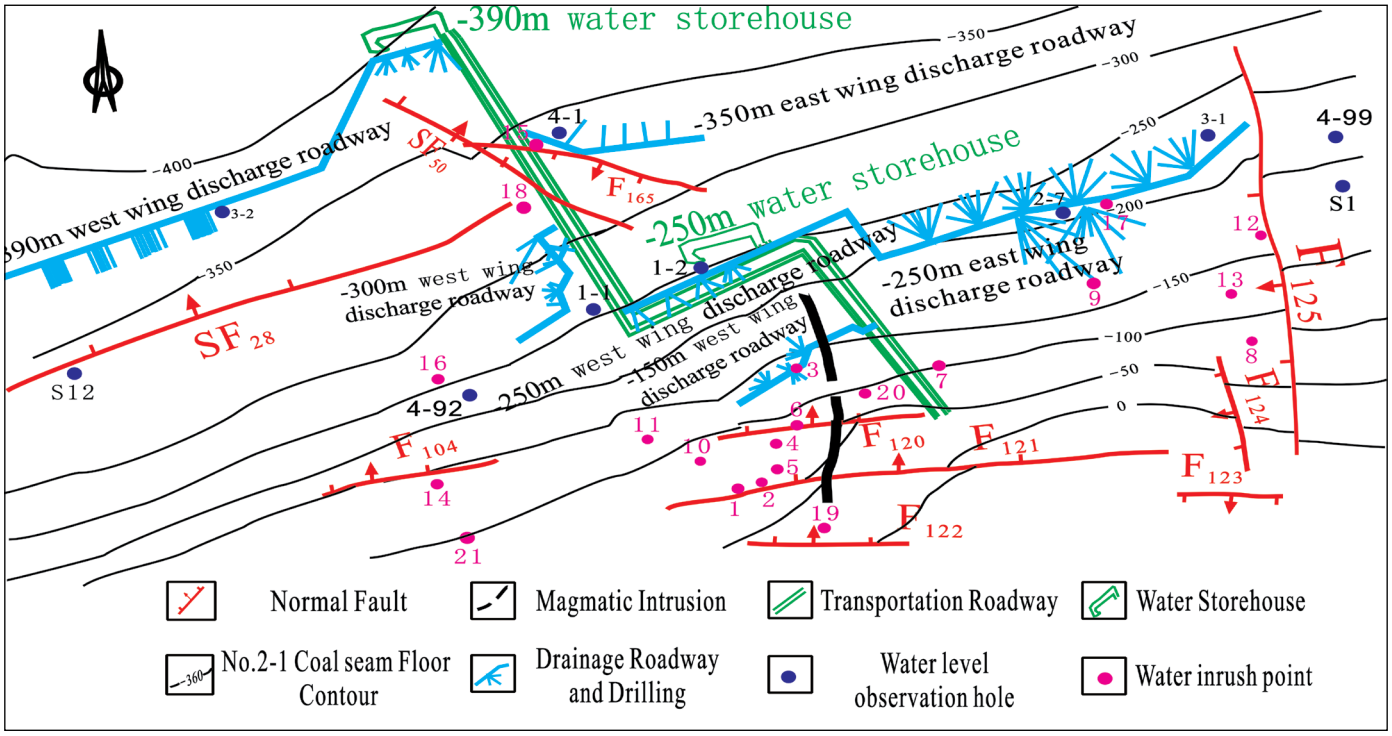

Figure 6. *Distribution map of draining lane and drilling hole of No. 1 well*

Table 3. *Summary statistics of water discharge in the draining lane*

Roadway	Drill hole			Water inflow (m^3/h)		
	Total	Number of water inrush	Proportion (%)	Minimum	Maximum	Mean
-150 m West Wing	9	9	100	16.00	150.00	90.00
-250 m West Wing	23	23	100	0.01	180.00	85.54
-250 m East Wing	18	18	100	0.50	232.00	84.28
-300 m West Wing	27	11	40.74	0.00	85.00	14.96
-350 m East Wing	5	5	100	1.00	3.00	2.00
-390 m West Wing	37	26	70.27	0.00	90.00	17.61

6. Analysis of time and space changes in the water level

The location of the groundwater level observation hole for the CL and its water level dynamic changes are shown in Figure 7.

From July 2000 to July 2006, the drainage of the No. 1 well mainly occurred in the -150 m West Wing and the -250 m West Wing discharge roadways, and the discharge volume was stable at 800 m^3/h. The 4-92 observation hole, which was close to the two discharge roadways, changed from +6.0 m to -210.0 m, and continued to decrease by 216 m. From July 2006 to March 2012, the main drainage was in the -250 m West Wing discharge roadway, the drainage water volume was 1373.5 m^3/h, and the water level of the 4-92 observation hole was basically stable at -220~-225 m. With the implementation of the hydrophobic scheme, the water in the East Wing -106 m water inrush point disappeared, indicating that the groundwater of the CL at the shallow elevation of -150 m and F_{125} fault was closely related to underground water.

From July 2006 to March 2012, while the -250 m West Wing drainage roadway was draining, drainage also occurred in the -250 m East Wing drainage roadway, with a drainage volume of 2,580.0 m^3/h. The water level of the 4-99 observation hole on the east side of the F125 fault decreased from -11.0 m to -42.2 m, or only 31.2 m. The water level of the S1 observation hole decreased from -29.2 m to -60.5 m, which only decreased by 31.3 m, reflecting the poor water conductivity of the F_{125} fault as a whole. These results showed that the groundwater hydraulic connection of the CL on both sides of the fault was not very close.

From April 2012 to September 2013, the water volume of the -250 m East Wing roadway remained steady at 500 m3/h, and the water levels of observation holes 2-7 and 3-1 (Figure 6) near the -250 m East Wing discharge roadway decreased from -162.5 m and -184.1 m to -232.4 m and -230.5 m, respectively, while the groundwater level tended to be consistent. These data indicate that the aquifer of the CL on the west side of the F_{125} fault was well connected. In addition, the water levels of 4-99 and S1 on the east side of the F_{125} fault were stable at -42.7 m and -66.8 m. Compared with holes 2-7 and 3-1 on the west side, the water level difference was above 160 m, which proved that the hydraulic connection of the groundwater in the CL on both sides of the F_{125} fault was not close (Wang, 2015). Additionally, there was a difference between the 4-99 and S1 water levels of the 386 m east side of the F_{125} fault is 24.1 m, indicating that the groundwater hydraulic connection of the CL in the east side of the F125 fault was not close.

From April 2012 to October 2015, a hydrophobic decompression project was carried out in the -300 m West Wing discharge roadway (Figure 6). The total hydrophobicity volume was 600 m3/h, and the water level of S12, 1-1, and 1-2 decreased from -244.8 m, -219.9 m, and -231.5 m to -310.0 m, -315.0, m and -305.4 m, respectively. As seen from Figure 6, the distances between S12 and the 1-1 and 1-2 holes were 1,000 m and 350 m, respectively, and the water level elevations of the three boreholes were basically the same in October 2015, which confirmed the hydraulic connection of the CL groundwater in the west part of the F_{125} fault and the shallow part of the elevation of -300 m is relatively close.

From May 2014 to May 2017, drilling holes were constructed along the -390 m West Wing discharge roadway and -350 m East Wing discharge roadway, and underground water drainage was performed. The drainage volume of the -350 m East Wing discharge roadway is only 3 m^3/h, the 4-1 water level remains at about -310 m, and there was little change, indicating that the groundwater hydraulic connection of the CL in the deep No. 1 well was not close.

7. Tracer tests under coal mine

In order to ascertain the hydraulic connection of the CL groundwater on the east and west sides of the F_{125} fault below the No. 1 well East Wing -150 m level, four tracer tests were carried out. The tracers were all potassium iodide (Zhao et al., 2016; Soulsby et al., 2016; Yu and Xu, 2013 Zhou et al., 2011). The interval between the two tests was more than 2 weeks. The input points were 4-99, S1, S9, and S2 on the east side of the F_{125} fault (Figure 8), and the receiving point was the 3-1 water level observation hole on the -250 m East Wing discharge roadway (Figure 8). Water samples were collected every 2 h at the receiving point and the potassium iodide content was measured on-site with a HI93718 portable iodine analyzer with a test accuracy of 0.1 mg/L. The test results

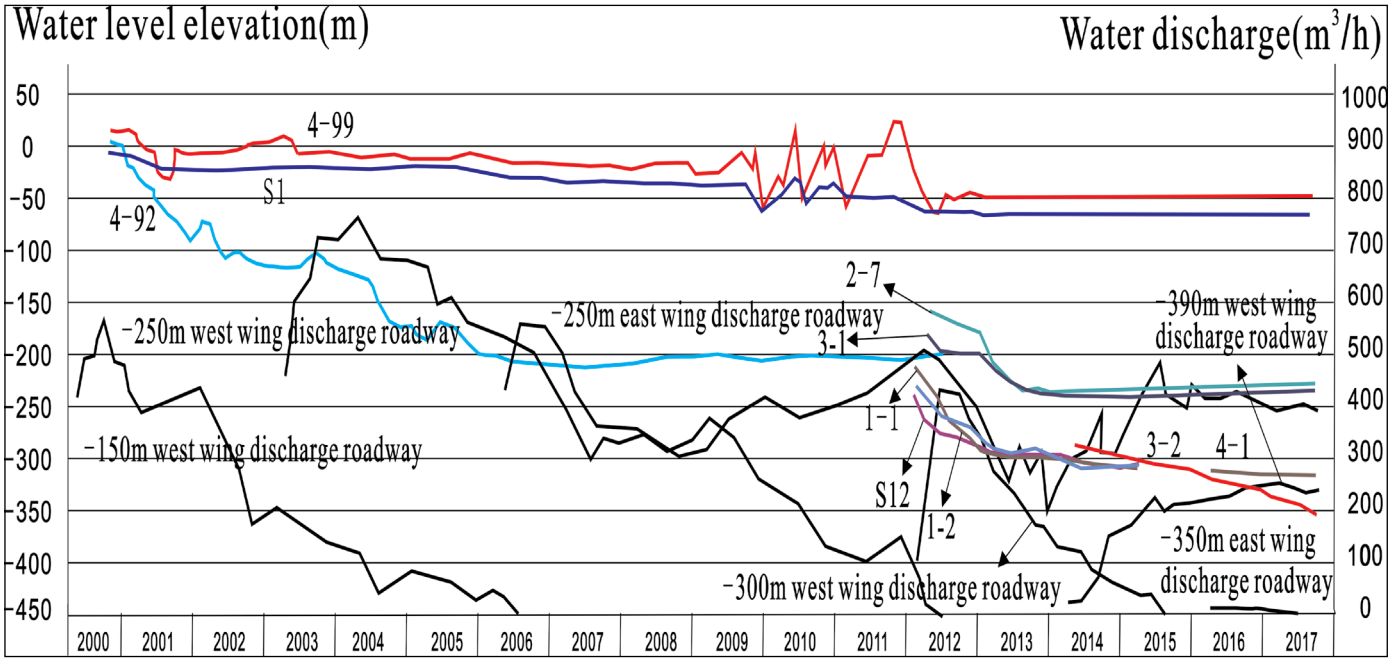

Figure 7. *Dynamic changes of water and water level in draining Lane of No. 1 well.*

The test results in Table 4 showed that only the potassium iodide at input point 4-99 was detected in the 4 tracer test, and it took 104 h to reach the -250 m East Wing discharge roadway receiving point beyond the 660 m distance. The calculated tracer migration rate was 6.3 m/h, indicating a weak hydraulic connection between them.

In addition, from Table 4 and Figure 8, we know that in the four-time tracing test, when 4-99 was the input point, the potassium iodide content was detected at the receiving point, and the other three tests (especially the S2 tracer test closer to the receiving point) did not detect potassium iodide contents at the receiving point, indicating that there was no obvious hydraulic connection between the three input points and the receiving point for the CL groundwater. The above tracer tests showed that the total hydraulic connection of the CL karst on both sides of the F_{125} fault below the No. 1 well East Wing -150 m were weak, and only a weak hydraulic connection was found in the local area, indicating the obvious difference in the karst space development of the CL.

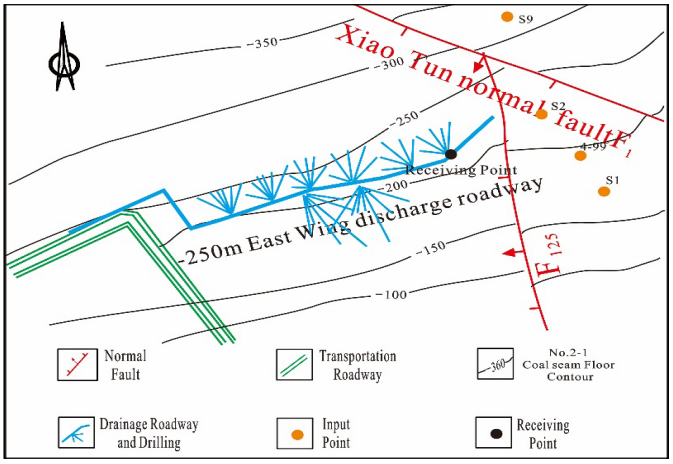

Figure 8. *Distribution map of input point and receiving point of tracer test*

Table 4. *Tracer test summary*

Input point	Test time	Input amount (kg)	Input concentration (mg/L)	Acceptance concentration (mg/L)	Collection days (d)	Number of water samples collected (group)	Input point and receiving point distance (m)	Arrival time (h)
4-99	2010/7/17 9:00 a.m.	5.00	1000	0.3	7	86	660.00	104
S1	2010/8/3 9:35 a.m.	5.00	1000	-	15	184	724.00	Not received
S9	2010/8/19 11:00 .m.	5.50	1100	-	9	87	913.00	Not received
S2	2010/9/15 10:00 .m.	4.50	900	-	21	120	540.00	Not received

Conclusions

The transient electromagnetic exploration results showed that the No. 1 well water-rich anomaly area was scattered, and the area was less than 20 % of the entire exploration area, indicating that the CL aquifer was weakly water-rich as a whole. The buried depths of 0~40 m and 40~80 m water-rich anomalies partially overlapped, reflecting a certain hydraulic connection between the shallow and deep groundwater of the CL aquifer. There were few water-rich anomalies near the F_1, F_5, F_{125}, and SF_{28} faults, which proved that these faults were poorly water-rich and water-conducting, making the deep karst water form an independent closed system.

The comprehensive study of hydrogeological exploration, water in-rush characteristics, and downhole drainage data showed that karst development in the shallow part of the CL aquifer was stronger than that in the deep part, showing vertical zoning. The water inrush in the shallow part at an elevation of -200 m accounted for 81.82 % of the total water inrush accidents. The water inrush volume exceeded 10 m^3/h, the CL aquifer accounted for 84.62 %, and the water inrush caused by geological structures accounted for 61.54 %, which was mainly concentrated near the small faults.

The spatio-temporal variation of the water level and the tracer test analysis showed that the hydraulic connections of the CL groundwater in the shallow part at -300 m and the west of the F_{125} fault were relatively close, but the groundwater hydraulic connection in the deep (elevation -390 m) CL was not close. The F_{125} fault had poor water conductivity overall, and there was a weak hydraulic connection between the CL groundwater found only in the fault zone at -200 m elevation; The CL groundwater in the eastern F_{125} fault did not have a close hydraulic connection.

Acknowledgements

This work was supported by the National Natural Science Foundation of China (Grant 41802186, 41972254), the Innovation Scientists and Technicians Troop Construction Projects of Henan Province (Grant CXTD2016053), the Fundamental Research Funds for the Universities of Henan Province (NSFRF200103).

References

Dai, G.L. 2010. The effect of geology structure on hydrogeology characteristics of Hancheng mining area. Journal of Arid Land Resources and Environment. vol. 24, no. 7, pp. 62-67.

Dai, Q.H., Peng, X.D., Yang, Z., Zhao, L.S. 2017. Runoff and erosion processes on bare slopes in the Karst Rocky Desertification Area. Catena. vol. 152, pp. 218-226.

Dong, S.N. 2010. Some key scientific problems on water hazards frequently happened in China's coal mines. Journal of China Coal Society. vol. 35, no. 1, pp. 66-71.

Hao, B.Y., Guo, Y.H., Wang, F., Zhang, H. 2013. Study on development features and major control factors of Ordovician limestone karst in Gujiao mining area. Coal Science and Technology. vol. 41, no. 2, pp. 91-95.

Hu. W.Y., Zheng, G., Yan, L.Y. 2010. Study on detecting deep karst developing features by chemical tracing. Carsologica Sinica. vol. 29, no. 2, pp.205-211.

Kovács A, Perrochet P, Darabos E, et al. 2017. Well hydrograph analysis for the characterisation of flow dynamics and conduit network geometry in a karst aquifer, Bükk Mountains, Hungary. Journal of Hydrology. vol. 530, no. 2, pp.484-499.

Lipar, M., Webb, J A. 2015. The formation of the pinnacle karst

in Pleistocene aeolian calcarenites (Tamala Limestone) in southwestern Australia. Earth-Science Reviews. vol. 42, no.4, pp.182-202.

Liu, B., Liu, Z.Y., Li, S.C., Nie, L.C., Su, M.X., Sun, H.F., Fan, K.R., Zhang, X.X., Pang, Y.H. 2017. Comprehensive surface geophysical investigation of karst caves ahead of the tunnel face: A case study in the Xiaoheyan section of the Water Supply Project from Songhua River, Jilin, China. Journal of Applied Geophysics. vol. 144, pp.37-39.

Qiao, W., Li, W.P., Zhang, X. 2014. Characteristic of water chemistry and hydrodynamics of deep karst and its influence on deep coal mining. Arabian Journal of Geosciences. vol. 7, no. 4, pp. 1261-1275.

Soulsby, C., Bradford, J, Dick, J, McNamara, J. P., Geris, J., Lessels, J., Blumstock, M., Tetzlaff, D. 2016. Using geophysical surveys to test tracer-based storage estimates in headwater catchments. Hydrological Processes. vol. 30, no.23, pp. 4434-4445.

Sun, L.L., Wang, Z.H., Wang, H.J., Wang, Y.H., Sun, Y.Q. 2013. Detection research on water abundance of floor aquifers. Mining Safety & Environmental Protection. vol. 40, no.1, pp.61-64.

Wang, Q., Wang, X.Y., Hou, Q.L. 2016a. Geothermal water at a coal mine: from risk to resource. Mine Water and the Environment. vol. 35, no. 3, pp. 294-301.

Wang, Q., Wang, X.Y., Liu, X.M., Zhen, X.G., Chen, G.S., Zhang, B. 2018. Prevention of groundwater disasters in coal seam floors based on TEM of cambrian limestone. Mine Water & the Environment. vol. 7, no. 2, pp. 300-311.

Wang, W.J. 2015. Research on water control effect of Xiatuanbai fault. Mining Safety & Environmental Protection. vol. 42, no.4, pp. 72-75.

Wang, X.Y., Ji, H.Y., Wang, Q., Liu, X.M., Huang, D., Yao, X.P., Chen, G.S. 2016b. Divisions based on groundwater chemical characteristics and discrimination of water inrush sources in the Pingdingshan coalfield. Environmental Earth Sciences. vol. 75, no. 10, pp. 1 -11.

Wang, X.Y., Zhao, W, Liu, X.M., Wang, T.T., Zhang, J.G., Guo, J.W., Cheng, G.S., Zhang, B. 2017. Identification of water inrush source from coalfield based on entropy weight-fuzzy variable set theory. Journal of China Coal Society, vol. 42, no. 9, pp. 2433-2439.

Wu, Q., Jia, X, Cao, D.T., Liang, Y.P. 2014. Impermeability evaluation method and its application on the ancient weathering crust of carbonatite in Middle Ordovician system in North China coalfield. Journal of China Coal Society. vol. 39, no. 8, pp. 1735-1741.

Wu, Q., Zhang, B., Zhao, W.D., Liu, S.Q. 2013. A new practical methodology of coal seam floor water burst evaluation: the comparison study among ANN, the weight of evidence and the logistic regression vulnerable index method based on GIS. Journal of China Coal Society. vol. 38, no. 1, pp. 21-26.

Yang, B.B., Yuan, J.H, Duan, L.H. 2018. Development of a system to assess vulnerability of flooding from water in karst aquifers induced by mining. Environmental Earth Sciences. vol. 77, no. 3, pp. 91

Yu, X.l., Xu, G.q. 2013. Connected experiment study on explore hydraulic connection between limestones in Panbei mine. Coal Science and Technology. vol. 41, no.10, pp. 105-107.

Zhao, L.J., Xia, R.Y., Yi, L.X., Yang, Y., Wang, Z., Liu, H.P. 2016. Quantitative analysis of the source and the effect of turbidity in karst river on tracer test. Acta Geoscientia Sinica. vol. 37, no.2, pp. 241-246.

Zhao, Q.B. 2014. Ordovician limestone karst water disaster regional advanced governance technology study and application. Journal of China Coal Society. vol. 39, no.6, pp. 1112-1117.

Zhou, C.X., Jiang, J.J., Dong, S.B., Yan, S.X., Chen, Y.M., Song, Y.X., Bian, J.M. 2011. Groundwater tracer test in Sanguikou Ore District, Wulate Houqi,Inner Mongolia. Journal of Jilin University (Earth Science Edition). vol. 41, pp. 285-292.